




TECHNICAL ARTICLE

Comparative Analysis of Structure and Properties of Nb-B Inoculated Direct Chill Cast AA4032 Alloy Extruded from As-Cast and Homogenized Conditions

NILAM S. BAREKAR ^{1,2,5} IVAN SKALICKY^{2,3} SHIHAO WANG,¹
PAVEL SHURKIN,¹ ONUH ADOLE,¹ N. HARI BABU,¹
and MARTIN JARRETT^{2,4}

1.—BCAST, Brunel University London, Uxbridge UB8 3PH, UK. 2.—Constellium University Technology Centre, Constellium UK Ltd., Brunel University London, Uxbridge UB8 3PH, UK. 3.—Constellium Extrusions Decin s.r.o, Ustecka 37, 405 35 Decin V, Czech Republic. 4.—Constellium UK Ltd, Grenville Court, Britwell Road, Burnham SL1 8DF, Bucks, UK. 5.—e-mail: n_barekar@yahoo.co.in

Al-Si wrought piston alloys can lack properties due to inefficient grain refining. A novel Al-Nb-B grain refiner was introduced some time ago, but has still not been assessed in industry for wrought alloys. This paper describes the first trial of Al-Ni-B addition and its impact on the full-scale manufacturing, structure, and properties of the AA4032 products extruded with and without billet homogenization. It is shown that Nb-B inoculation gives opportunities not only to have a refined as-cast structure but also a more homogenous distribution of the solute. In contrast, homogenization drives nucleation and coarsening of the Mg₂Si phase that is retained during further extrusion and heat treatment also affecting the precipitation and properties. It was observed that non-homogenized specimens perform better during machining and tensile testing compared to homogenized specimens. The results are supported by electron microscopy investigations of microstructure formation during different steps in downstream processing.

INTRODUCTION

Wrought heat-treatable 4xxx piston Al alloys are well-established engineering materials manufactured under tailored routes to exhibit a favorable set of mechanical and service properties. They begin their life cycle with direct chill (DC) casting to produce billets, followed by downstream thermomechanical processing, including direct forging or extrusion and precipitation treatment.^{1,2} Primarily, the latter should provide sufficient hardening governed by metastable precursors of the Mg₂Si and Q phases with high number density.³ Additionally, during the whole cycle, the shape and uniformity of hard insoluble constituents, such as Si, γ -Al₇Cu₄Ni,

δ -Al₃CuNi, and β -Al₉Fe₂Si₂, should be controlled to provide appropriate machinability upon cutting to a piston-like (or other) shape.^{4–6}

For tuning the above-mentioned structural features, grain refinement is the first procedure applied upon casting the wrought Al alloys. Ideally, a cast billet should have uniform fine grains and cell structure over its cross-section, no coarse intermetallics, minimum surface segregation, or shell zone, and an acceptable surface finish. The quality of the billet has a strong influence on the alloy response to the subsequent thermomechanical treatment.⁷ Apparently, as eutectic-formers, neither Si and Cu nor Fe and Ni, main components in the AA4032 alloy, are efficient agents for grain refining.^{8,9} At the same time, the Al-Ti-B grain refiner, which is well established in DC casting of wrought alloys, is poorly active on alloys containing more than 5 wt.% Si, due to the interaction of Ti with Si

followed by the formation of titanium silicides (i.e., TiSi , TiSi_2 , and Ti_5Si_3) and Ti-depletion in the melt.^{10,11}

One school of thought proposes manipulating the solidification instead by techniques involving direct melt shearing or ultrasonic treatment, both of which provide significant grain refinement, but still require substantial process improvements and upscaling before being implemented in industrial practice.^{12,13} Another method based on conventional chemical inoculation implies the design of special Ti-free grain refiners to avoid the Si poisoning effect. For instance, Al-B grain refiners have been shown to reduce grain size due to the high-nucleus potency of the AlB_2 particles.¹⁴ However, the Al-B grain refiner acts similarly to Al-Ti-B even if a minor amount of Ti is present in the alloy,¹⁵ which brings limitations in its use in large-scale manufacturing involving secondary scrap. Recently, Al-Nb-B and Al-V-B have been proposed as an alternative grain refining addition to overcome the Si poisoning effect. It should be noted that, in the case of the Al-Nb-B grain refiner, the Al_3Nb , NbB_2 , and NbB_3 particles are acting synergistically during solidification,^{15,16} i.e., realizing the full potential of Nb and B, as compared to Al-V-B, in which only VB_2 particles are potent rather than Al_3V .¹⁷ Moreover, Nb-based master alloys have been found to be efficient over a wide range of compositions and solidification conditions.¹⁸

However, despite that manifest impact, Al-Nb-B grain refiners have not yet been fully studied in industrially important DC casting followed by thermomechanical treatment. One should note that inoculation by grain refiners might be able to tune not only primary fcc Al grains but also second-phase particles. This effect was evidenced for AlFeSi intermetallics in AA6xxx alloys inoculated by Al-Ti-B, and attributed to enhancing nucleation that occurred preferentially on the {0001} basal planes of TiB_2 .^{19,20} In the AA4032 alloy, the dominating possible stress raisers are coarse eutectic Si phase particles. In pivotal works on Al-Nb-B grain refinement, a considerably fine and homogeneous distribution of Al-Si eutectic was obtained due to a more uniform distribution of the alloying elements at the solidification front and eutectic pools as compared to the non-inoculated alloy.¹⁶ Similar results have been reported on the LM series Al alloys, including hypereutectic and insoluble intermetallics-rich compositions.¹⁸ Major experimental studies have been carried out using a TP-1 mold that had been established to simulate DC casting solidification conditions and to estimate grain-refining efficiency. However, according to,²¹ the shape and distribution of second phases are not consistent with DC casting, as these features also depend on other metallurgical factors, such as thermal gradients and macro-segregation of elements, etc. Therefore, it is expedient to conduct studies on large-scale DC-cast billets.

Grain refining can in some cases perform the function of a homogenization treatment. Meanwhile, to refine second-phase particles appropriately, homogenization is carried out at relatively high temperatures (commonly more than 550°C) and exposure times (commonly more than 5 h) that according to estimations requires up to 20%²² of the total energy consumed in the manufacturing of wrought products. For this reason, the idea of eliminating homogenization is appealing. This work aims to investigate and discuss the distinct features of the structure and properties of a DC-cast AA4032 alloy manufactured with and without the use of a NbB grain refiner and with or without homogenization before extrusion-based thermomechanical treatment.

EXPERIMENTAL PROCEDURE

Casting Procedure and Analysis of Grain Refining

Round billets of 152 mm diameter were cast in a pilot DC casting facility at the Advanced Metal Casting Centre in Brunel University, London. The DC caster consists of an electrical resistance tilting furnace (capacity up to 350 kg of liquid aluminum); a launder that provides a delivery system; two hot-top molds fitted into a casting pit; a hydraulic movement mechanism for ingots (with a maximum length of 2000 mm); a displacement sensor for measuring the casting length and speed; a submersible water pump; and a system of pipes and valves enabling water-flow rates of between 1 l/s and 3 l/s for the two molds. Process parameters such as melt temperature in the launder, water flow rates, and casting speed were controlled and recorded as 1000 K, 3 mm/s and 3 l/s, respectively. The casting procedure started with the preparation of the AA4032 alloy (concentration in wt.%, Al-12Si-1.2Cu-1.1Mg-0.5Fe-1Ni) by melting the primary material, the master alloys, and then adding the grain refiner in the form of an Al-4Nb-0.5B rod to have an effective Nb content of 0.1 wt.%, according to Ref. 18. A steady-state was reached after a sufficient length of the billet was produced (~300 mm). Cast billets were cut by sawing at transverse sections from the steady-state stage.

The sawed slices were cut to smaller samples, which were then ground and polished. The grain structure was analyzed under cross-polarized light after anodizing the samples in a 3% HBF_4 aqueous solution. Non-treated AA4032 (hereafter, NT) alloy and an alloy inoculated with the Al-3Ti-1B master alloy were used as references to compare the efficiency of the Nb-B grain refiner. The cooling curves were recorded by thermal analysis.

Downstream Processing

One batch of AA4032 as-cast billets was homogenized before extrusion and a second batch was not

homogenized (i.e., was investigated in the as-cast condition). Both batches were extruded to 33-mm-diameter round bars by hot extrusion using a 1.6-MN extrusion press at the Advanced Metal Casting Centre (AMCC) at Brunel University, and then hardened by cooling with water immediately after extrusion. The maximum extrusion breakthrough pressure for the non-homogenized billets was 10% more than the homogenized billets. It is well established that homogenized billets extrude more easily and faster than as-cast billets.² The standard heat treatment T6 (peak aged)²³ was carried out with a batch of bars. To investigate the effect of separate solutionizing, another batch of bars was put in a temper T5 condition, i.e., aged straightaway after extrusion without any solution treatment.

Examination of Samples

The microstructures were analyzed using a Zeiss Supra 35 field-emission gun scanning electron microscope (SEM) equipped with energy-dispersive x-ray analysis (EDX) and operating at 20 kV. Hardening precipitates were observed using a JEOL-2100F transmission electron microscope (TEM) operated at 200 kV. TEM specimens were first mechanically ground and polished to a thickness of 120 μm , and then punched into 3-mm disks. The disks were perforated by twin-jet electro-polishing with an electrolyte consisting of 1/3 HNO_3 in methanol below -25°C at an operating voltage of 20 V. All TEM observations were performed along the $\langle 001 \rangle_{\text{Al}}$ zone axis. The electrical conductivity of the as-cast and homogenized samples was measured with a Sigma Test Unit for the evaluation of the dissolution process of the alloying elements. Brinell hardness measurements were carried out on the as-cast and homogenized samples using a load of 62.5 N and a ball diameter of 2.5 mm. Tensile tests were conducted on at least 4 samples using an Instron 5559 universal electromechanical testing machine according to ASTM E8, with dual-rate (with a strain rate of 2.5×10^{-4} /s to 1% strain and then 6.6×10^{-3} /s to failure).

RESULTS AND DISCUSSION

As-Cast and Homogenized Microstructure

Figure 1 shows the cooling curves and representative microstructures observed with polarized light, which together make it possible to deduce the grain-refining efficiency. From the cooling curves, it is apparent that Al-4Nb-0.5B induces heterogeneous nucleation of (Al) to the highest extent ($\Delta T = 0.4$ K) in comparison with Al-3Ti-B ($\Delta T = 1.2$ K) and with the NT alloy ($\Delta T = 3.5$ K). This signifies that nucleation of the first fractions of solid (Al) phase takes place more easily in the AA4032 alloy inoculated with Al-Nb-B.²⁴ This phenomenon well explains the substantial decrease in grain size produced by inoculation with Al-Nb-B.

Unlike the billets produced by commercial practice, i.e., by the addition of Al-3Ti-1B, the billets produced by Al-4Nb-0.5B show a fine nearly equiaxed structure from the edge to the center of the billet. The average grain size for billets refined by Al-4Nb-0.5B was 300 ± 46 μm , showing slight deviations depending on the local chemical composition and cooling rate in different parts of the billet. The local cooling rate (dT/dt) encountered in a commercial size DC-cast ingot varies from 0.4 K/s in the center of the billet to around 10 K/s in the surface zone.²⁵ Despite a slightly larger grain size in the center (about 340 μm), it is still advantageously smaller than even that in low-Si alloys like AA319 (Al-6%Si-4%Cu) inoculated with Al-Ti-B, which was reported in Ref. 26 to have a grain size of around 400 μm after double Al-5Ti-1B addition. Ultimately, the efficiency of the Al-4Nb-0.5B master alloy in grain refining during large-scale DC casting has been demonstrated here for the first time. Following the established understanding of structure formation during DC casting,²⁷ and work²⁸ that discussed the formation of the directionally solidified structure of Al-10Si alloy treated with Al-Nb-B, constrained growth of columnar grains is provided by the Nb-based grain refiner, and numerous nucleation sites lead to mutual growth restriction among the growing grains.

The black areas in the grain structure correspond to eutectic pockets that are much smaller in the case of the billet refined by Al-4Nb-0.5B, as compared to the conventional practice. Microstructural features are generally consistent with the conventional DC-cast AA4032 alloy structure discussed in Ref. 4. In the as-cast state, there is a low number of secondary dendritic arms that leave the eutectic mixture surrounding the nearly equiaxed primary (Al) dendritic cells. In addition, there are ultrafine eutectic (Si) bands which, however, switched to discrete particles with a rounded shape most likely due to spheroidization followed by advanced coalescence to nearly 10 μm after high-temperature annealing. In other words, while both structures look homogeneous, microstructural features such as grain size and Si-rich eutectic allow us to speculate about comparable processability during deformation, as less energy must be required for redistributing ultrafine eutectic (Si) as compared to breaking up large, round particles. Among other constituents, compounds containing Ni, Cu, and Fe do not show pronounced changes in their shape after homogenization. Even though the intermetallics partially broke up, most of them retained a flake-like shape that can be explained by the much lower diffusion coefficients of Fe, Ni, and Cu as compared to Si.

Figure 2 shows the SEM back-scattered images and the EDX line-scan analysis conducted on as-cast and homogenized AA4032 samples. The microstructure of the as-cast billet consisted of primary dendrites of aluminum-rich solid solution, eutectic, and a well-defined interdendritic network

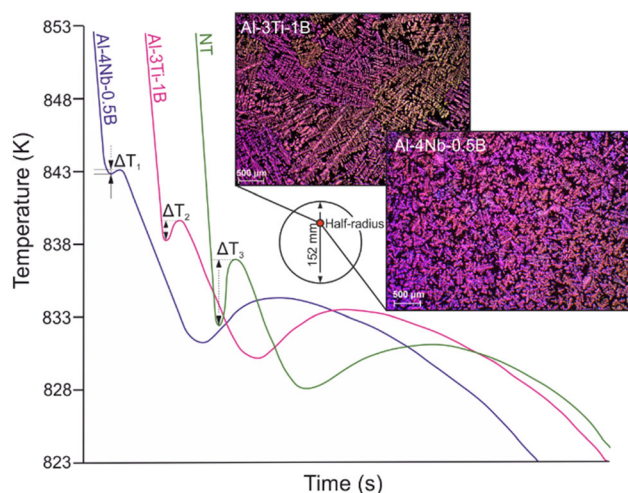


Fig 1. Efficiency of grain refining by Al-4Nb-0.5B in the present study compared to Al-3Ti-1B and non-treated (NT) alloy.

of intermetallics (Fig. 2a). After homogenization, the intermetallics broke up into relatively small discrete particles. The interdendritic platelets were replaced almost entirely by discrete, round particles, giving a 'necklace' type configuration (Fig. 2b). The size and distribution of the Mg_2Si phase (black constituents in Fig. 2a and b that influence precipitation hardening of the extruded products are drastically different in the as-cast and homogenized billets. The result of EDX line-scan analysis conducted on the as-cast sample (Fig. 2c) did not reveal any segregation of Mg and Si in the microstructure. This is attributed to the uniform microstructure achieved by the use of the efficient Al-4Nb-0.5B grain refiner, and might be due to a high enough cooling rate during solidification of the billet that retained the alloying elements in solid solution.²⁹ Similar findings were observed in Ref. 30 focused on DC casting and the compressive deformation of the AA4032 alloy with Er addition. On the other hand, EDX line-scan analysis conducted on the homogenized sample (Fig. 2d) revealed the segregation of Mg and Si associated with the secondary phases. They likely appeared as a result of secondary precipitation of the Mg_2Si during post-homogenization cooling.³¹ Therefore, significant levels of Mg and Si will not be available to form the strengthening precipitates during aging. It is possible that, due to the high refining efficiency of the Al-Nb-B grain refiner, a reduced total solidification time promoted a finer distribution of phases, a cellular dendritic structure, and the formation of a supersaturated solid solution during accelerated solidification.²⁶ Additionally, due to low dendrite diameters, there is a shorter path for Mg, Si, and Cu atoms to travel and achieve equilibrium, and probably more time for Mg_2Si to nucleate and grow. The higher amounts of Mg and Si atoms in the solid solution of the as-cast sample as compared to the homogenized sample were also reflected by lower conductivity (18 MS/m

versus 24 MS/m) and higher hardness (100 HV versus 70 HV). This also clarifies the higher extrusion breakthrough pressure for the non-homogenized billets, which we believe is worth considering for the sake of the elimination of costly homogenization treatment.

Extruded and heat-treated microstructure

The representative SEM back-scattered microstructures of the AA4032 alloy after extrusion of as-cast and homogenized billets in the initial (T1), T5, and T6 conditions are shown in Fig. 3. As described previously, Al-Nb-B inoculation had an effect on the as-cast microstructure and may provide better processability during extrusion. However, in the extruded condition, its effect should be negligible, as other factors, like deformation-induced energy and annihilation of the microstructure, play a major role in structure formation. Specifically, during extrusion, the structure encountered heating and deformation, both of which led to the appearance of an oriented structure decorated by undissolved particles. The presence of the black Mg_2Si phase constituents (arrowed in the insets of Fig. 3) can be observed in all studied conditions, but their amount and size are significantly different. The sample extruded from the as-cast condition hardly shows any Mg_2Si inclusions (Fig. 3a). There is no further coarsening of the Mg_2Si particles which occurred in the sample extruded from the homogenized condition (Fig. 3b). It is most likely that the low exposure time, during heating before extrusion and friction while processing, both act to suppress significant coarsening of Mg_2Si . At the macro-scale level, there is no significant difference between the T1 and T5 conditions in both the samples extruded from different billets (Fig. 3c and d). In contrast, separate solution treatment drove the precipitation of the Mg_2Si phase (Fig. 3e) in the sample extruded from the as-cast condition that might be associated with the appearance of preferential nucleation sites with relatively higher energy stored during deformation. Meanwhile, in the homogenized T6 sample (Fig. 3f), these precipitates are larger with a higher volume fraction.

Figure 4 shows the comparison in the size distribution of the black phases between T6-conditioned extruded bars manufactured from as-cast and homogenized billets. One should note that the black particles that appeared after T6 treatment in the non-homogenized extruded sample have a dominating size of roughly 1–1.5 μm and there are no particles more than 3.5 μm . Meanwhile, the sample extruded from the homogenized billet shows particles of up to 6 μm , which is equal to the size of other insoluble intermetallics present in the microstructure. Apparently, there should be a difference in the response to precipitation treatment among samples based on the different solubility of the main elements, Si, Mg, and Cu.

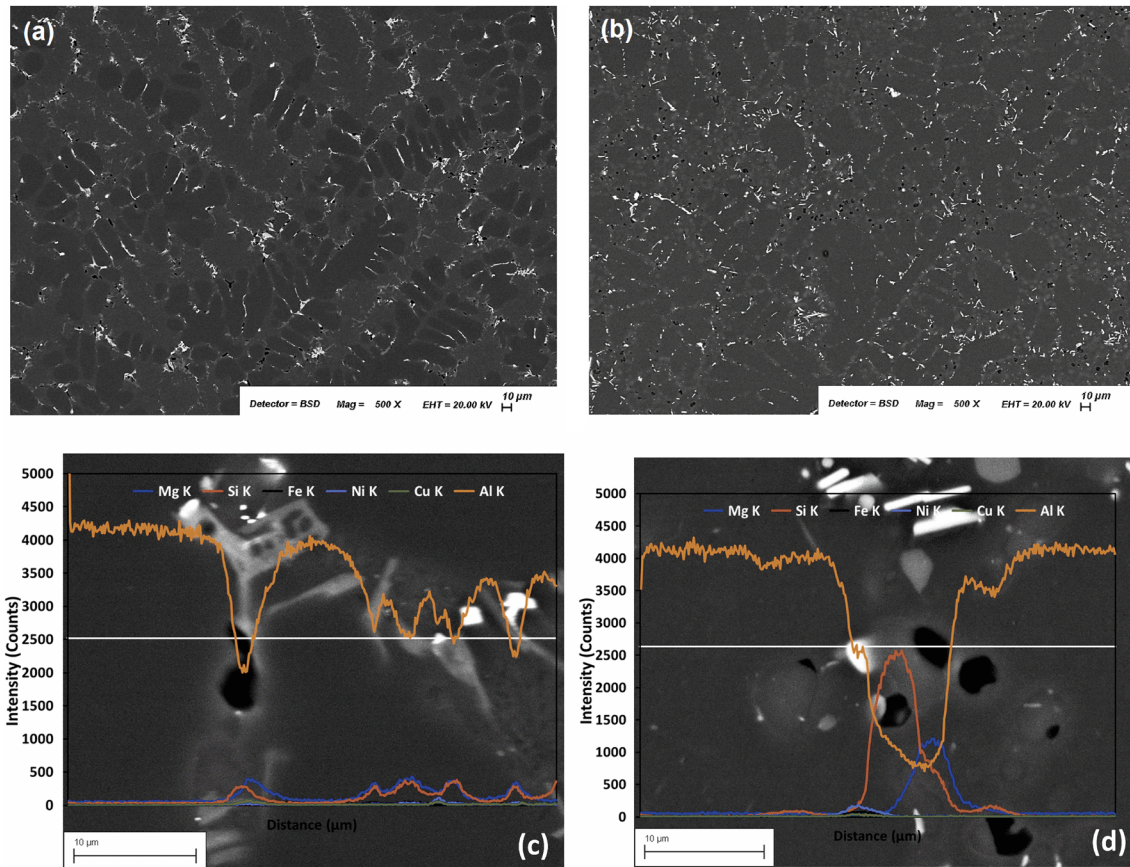


Fig 2. SEM micrographs of the AA4032 alloy in as-cast (a) and as-homogenized condition (b), and EDS scan results obtained from the as-cast (c) and as-homogenized (d) samples.

To estimate the possible differences in the phase composition, Thermo-Calc software (TCAL4 database) was used,³² and two states reflecting microstructures of the bars extruded from the non-homogenized and homogenized billets were considered. As observed from Fig. 3a and b, the Mg_2Si phase is hardly visible in the bar extruded from the non-homogenized billet, whereas it is clearly visible in the bar extruded from the homogenized billet. For this reason, we calculated the phase composition at 803 K (temperature at the end of extrusion) with and without the appearance of the Mg_2Si phase (Supplementary Table 1).

Phase composition presented in the Supplementary Table 1 is consistent with previous work on the 4032 alloy,³⁰ and also with the phase composition of multicomponent Al-Si piston alloys.³³ One should note that the Mg, Si, and Cu content in the fcc (Al) is consumed not only by Mg_2Si phase but also by the eutectic (Si) and Fe- and Ni-bearing phases, which were observed in the BSD images presented in Figs. 2 and 3. Meanwhile, after excluding Mg_2Si from the calculation, only the Mg content is increased (from 0.63 wt.% to 0.76 wt.%) while free silicon is consumed mainly by eutectic (Si). The latter shows an increase in volume fraction from 11.05 vol.% to 11.11 vol.% after excluding Mg_2Si

from the calculation. Usage of an equilibrium phase diagram can be misleading in predicting phase composition during precipitation, due to the kinetic-controlled and non-equilibrium nature of the process. However, it can give us a clue about the equilibrium phase composition which can be achieved at the final stage of precipitation. According to the results presented in the Supplementary Table 2, there is a decrease in Si and an increase in the Q phase in the bar extruded from the non-homogenized billet. Moreover, the change caused phase composition of the solid solution to fall in the area with Mg_2Si , which is the stable phase for β'' and β' precursors.

One should note that β'' are the main precipitates in the peak-aged AlMgSi(Cu) alloys.^{34,35} Due to the larger size, weaker strain fields, and broadening precipitation length distribution, their transformations into other lath-like Q phase precursors is associated with a reduction in the mechanical strength.^{36,37} Different studies give controversial information on the type of precipitates in AA4032 alloy.^{3,30} For this reason, it is essential to carry out experimental investigations with TEM.

TEM investigations of the T6 tempered samples are shown in Figs. 5 and 6. Most of the precipitates in the peak-aged condition for the homogenized and

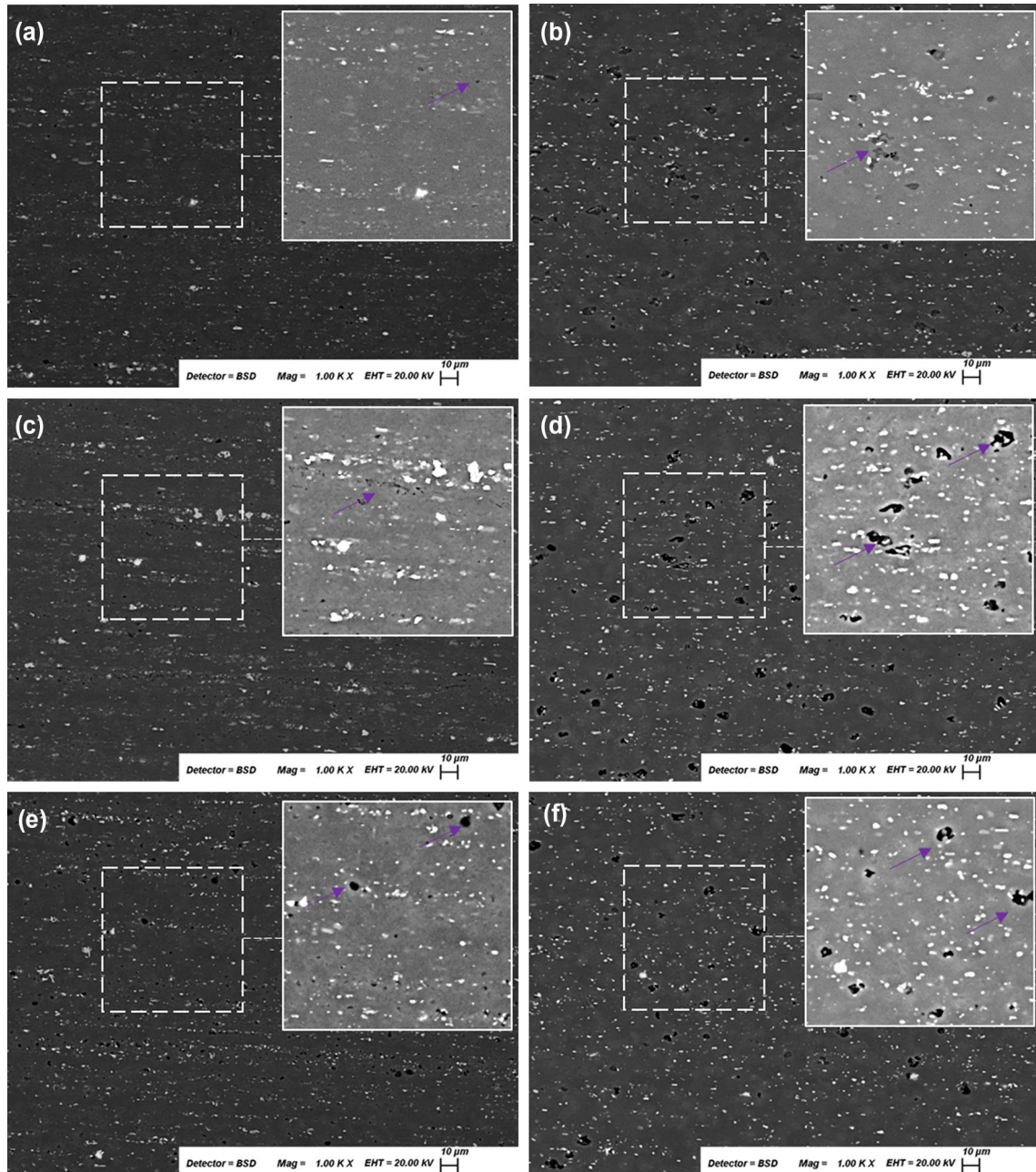


Fig 3. SEM micrographs of the AA4032 extruded products: (a) extruded from as-cast condition T1, (b) extruded from homogenized condition T1, (c) extruded from as-cast condition T5, (d) extruded from homogenized condition T5, (e) extruded from as-cast condition T6, and (f) extruded from homogenized condition T6.

non-homogenized samples are needle-like β'' precipitates aligned along $\langle 001 \rangle_{Al}$. A minority of lath-like precipitates were observed in both samples. They may be L or QC phases according to their characteristic habit planes parallel to $\{100\}_{Al}$ or $\{510\}_{Al}$. The high-resolution TEM images in Fig. 5 reveal typical edge-on β''^{34} and L precipitates.³⁵ With Al as reference, β'' exhibits a monoclinic unit cell structure of $a = 1.516$ nm, $c = 0.674$ nm, and $\beta = 105.3^\circ$, as shown in Fig. 5a, with the following orientation relationship to the matrix: $(010)\beta'' // (001)_{Al}$, $[100]\beta'' // [-230]_{Al}$, $[001]\beta'' // [310]_{Al}$. L phase

exhibits a monoclinic unit cell with parameters $a = 1.032$ nm, $b = 0.81$ nm, and $\gamma = 101^\circ$, as shown in Fig. 5b. Although the number density of the precipitates appears to be higher in the non-homogenized sample, it was not possible to compare the homogenized and non-homogenized samples properly without making allowance for the different thicknesses of the two specimens. Assuming a similar thickness, the area density of the precipitates between the two specimens suggest that the number density of the precipitates in a given area of the non-homogenized condition is higher. However,

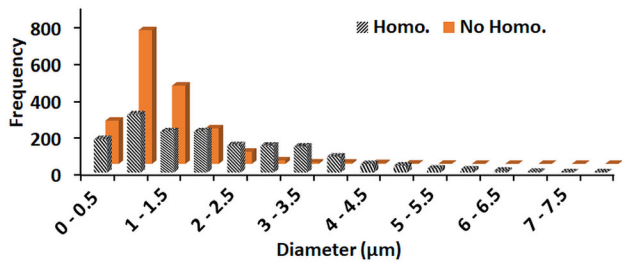


Fig 4. The size distribution of Mg₂Si phase present in the AA4032 extruded products.

it was noticed that lath-like precipitates occupy in a relatively higher proportion in the homogenized sample than in the non-homogenized sample. Measurement of the number of edge-on precipitates in both samples revealed that there were a smaller proportion of lath-like precipitates in the non-homogenized sample (5 out of 138) than in the homogenized sample (5 out of 35).

The effect of the precipitates on the strength of the aluminum alloys at the onset of yielding can be predicted by the Orowan equation in its simplest form: $\tau = Gb/\lambda$, where G is the shear modulus, b is Burgers vector of dislocation, and λ is interparticle spacing.³⁸ From Fig. 5, it can be noticed that the distance between the precipitates is smaller in the case of the non-homogenized material. Smaller interparticle spacing in the case of the non-homogenized material should therefore result in a higher strength compared with the homogenized material.

Machinability and Tensile Properties

Chip breakability in terms of the number of chips per 100 g is shown in Fig. 7 for the T5 and T6 samples extruded from as-cast and homogenized AA4032 materials. This indicator of machinability for the AA4032 homogenized T6 specimen is approximately 50% higher than for the homogenized T5 specimen. Similarly, the machinability of the AA4032 non-homogenized T6 specimen is approximately 80% higher than for the non-homogenized T5 specimen, while the machinability indicator for the AA4032 non-homogenized T6 specimen is approximately 35% higher than for the homogenized T6 specimen. A large number of chips for the non-homogenized sample indicates that a relatively smaller chip size was being produced during machining compared with the homogenized sample. The reason for the advantageous properties of the bar produced from the non-homogenized billet is likely to be a fine and uniform distribution of insoluble particles within the matrix. These finely dispersed phases particles assist the formation of short, broken chips, regardless of where the tool contacts the article being machined.⁶ It should be noted that this bar contains far fewer and finer-scale black Mg₂Si particles as compared to the homogenized material. The Mg₂Si particles are known for their hardness and brittleness and for

acting as stress raisers.³⁹ During turning, extensive plastic deformation occurs in the shear plane, which causes the shear failure of less ductile materials.⁴⁰ Furthermore, because there is a different hardness and different thermal expansion of the secondary phases and the matrix, the secondary phase particles can act as a source of stress concentration, leading to crack formation.

Table I shows a comparison of the tensile properties of the extruded bars of AA4032. Compared with the conventional homogenized material, the non-homogenized material shows a higher yield strength, ultimate tensile strength, and lower elongation. The aged (T5) specimens showed a relatively lower yield and ultimate tensile strength when compared with the solutionized and aged (T6) specimens. The results are consistent with the microstructural analysis. Specifically, in the T6 condition, separate solution treatment probably caused additional Cu dissolution in both samples, leading to a higher strength compared with the T5 condition. The different Mg and Si contents changed the precipitation sequence, as described in the previous section, and led to increased strength in the non-homogenized material. Although the non-homogenized material shows a slightly lower elongation, it still has a ductility acceptable for piston application, with overall better properties than in the as-cast material.³³

CONCLUSION

The use of an Al-Nb-B grain refiner in AA4032 DC-cast billets leads to finer-scale grain sizes, finer-scale secondary phase particles, and changes in precipitation hardening behavior, all of which enable the elimination of homogenization in the downstream processing of the AA4032 alloy, providing overall a better combination of the essential material properties of machinability, mechanical strength, and ductility. The reasons for these effects have been investigated in detail, and the main detailed conclusions are formulated as follows:

1. AA4032 alloy inoculated with Al-4Nb-0.5B alloy was successfully manufactured by industrial-scale DC casting for the first time. A pronounced effect of Nb-B inoculation was shown in the refining of grain structure and intermetallics and in the homogeneity of solute distribution.
2. In the as-cast condition, most of the Mg and Si is in solid solution as a result of an accelerated cooling rate, probably caused by efficient inoculation. In contrast, after homogenization, Mg₂Si discrete particles appeared, caused by secondary precipitation during post-homogenization cooling. The as-cast material, therefore, shows a lower electrical conductivity and higher hardness.
3. As-cast and homogenized billets were successfully extruded to bars. The microstructure of the homogenized extruded products showed the

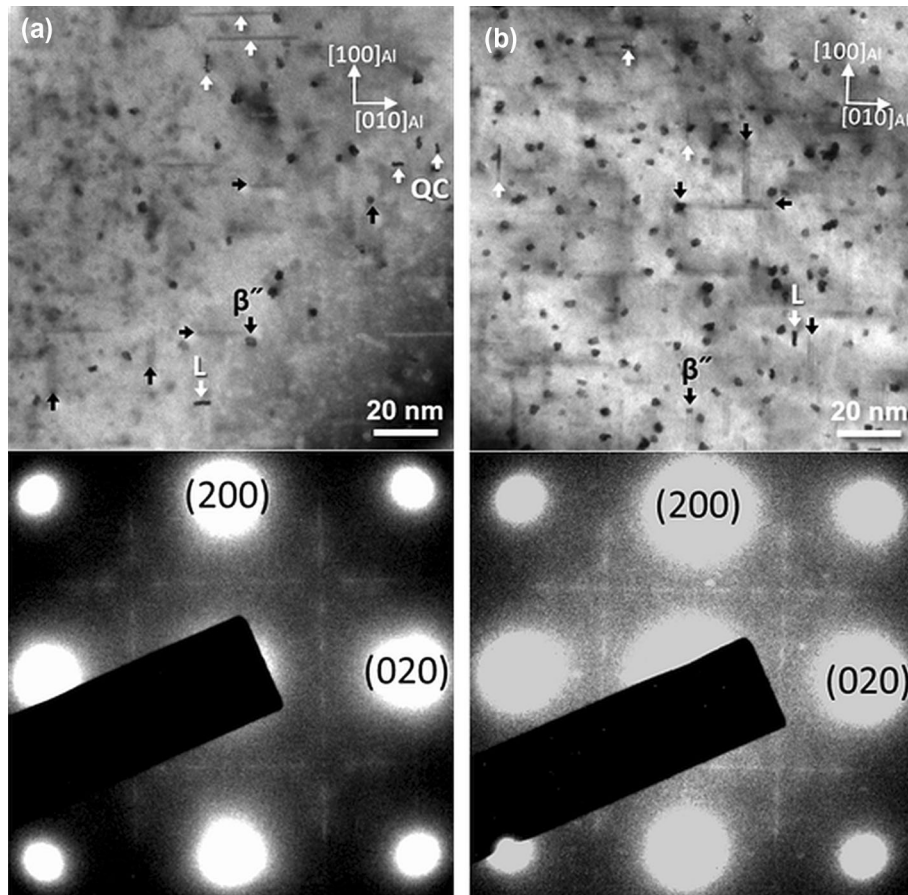


Fig 5. Bright-field TEM images of T6-tempered AA4032 extrudates taken with the electron beam along the $\langle 100 \rangle_{Al}$ orientation: (a) homogenized and b) non-homogenized. Needle-like β'' and lath-like L/QC phases are marked with *dark* and *white* arrows, respectively.

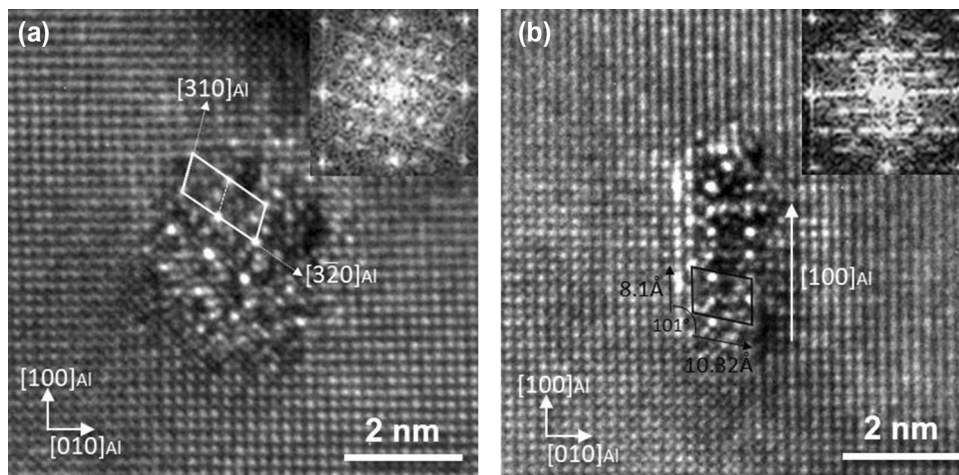


Fig 6. HRTEM images showing the typical edge-on (a) needle-like β'' and (b) lath-like L precipitates, with the corresponding fast Fourier transformation patterns inserted.

presence of larger Mg_2Si particles in all conditions, i.e., T1, T5, and T6 compared with the non-homogenized material.

4. In T5 and T6 conditions, the machinability and

tensile yield strength of the non-homogenized material are better than in the homogenized material because of the absence of the brittle Mg_2Si phase and a modified precipitation se-

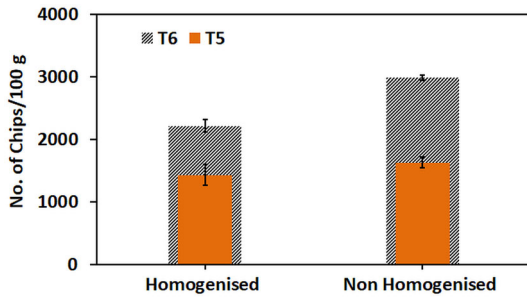


Fig 7. Machinability in terms of chip weight at a cutting speed of 2.35 m/s and a depth of cut of 2 mm for AA4032 extruded from as-cast and homogenized billets followed by T5 and T6 treatment.

Table I. Mechanical properties of the AA4032 extruded products in T5 and T6 conditions

Designation	YS (MPa)	UTS (MPa)	Elongation (%)
Homogenized T6	398 ± 4	432 ± 3	6.4
Non-homogenized T6	415 ± 3	451 ± 2	5.6
Homogenized T5	354 ± 4	409 ± 2	7.3
Non-homogenized T5	383 ± 3	433 ± 3	4.8

YS Yield strength, UTS ultimate tensile strength.

quence. The latter is caused by a different Mg/Si/Cu ratio in the primary fcc (Al) solid solution, which leads to a higher density of β'' precipitates with lower inter-particle spacing compared with the homogenized material.

ACKNOWLEDGEMENTS

The authors acknowledge the financial support of the UK Engineering and Physical Science Research Council (EPSRC Grant: The Future Liquid Metal Engineering Research Hub, under grant number EP/N007638/1) and Constellium.

FUNDING

Funding was provided by Engineering and Physical Sciences Research Council (Grant No. EP/N007638/1).

CONFLICT OF INTEREST

On behalf of all authors, the corresponding author states that there is no conflict of interest.

OPEN ACCESS

This article is licensed under a Creative Commons Attribution 4.0 International License, which permits use, sharing, adaptation, distribution and

reproduction in any medium or format, as long as you give appropriate credit to the original author(s) and the source, provide a link to the Creative Commons licence, and indicate if changes were made. The images or other third party material in this article are included in the article's Creative Commons licence, unless indicated otherwise in a credit line to the material. If material is not included in the article's Creative Commons licence and your intended use is not permitted by statutory regulation or exceeds the permitted use, you will need to obtain permission directly from the copyright holder. To view a copy of this licence, visit <http://creativecommons.org/licenses/by/4.0/>.

SUPPLEMENTARY INFORMATION

The online version contains supplementary material available at <https://doi.org/10.1007/s11837-021-05134-7>.

REFERENCES

- H.E. Hu, X. Wang, and L. Deng, *Mater. Sci. Eng. A* 576, 45. (2013).
- T. Sheppard, Metallurgical features affecting the extrusion of aluminium alloys. In: *Extrusion of Aluminium Alloys* (Springer: Boston, MA, 1999) p. 69-126.
- G. Biroli, G. Caglioti, L. Martini, and G. Riontino, *Scr. Mater.* 39, 197. (1998).
- S. Chankitmongkol, D.G. Eskin, and C. Limmaneevichitr, *Metall. Mater. Trans. A* 51, 818. (2020).
- Y. Zedan, F.H. Samuel, A.M. Samuel, and H.W. Doty, *J. Mater. Process. Technol.* 210, 245. (2010).
- N.S. Barekar, I. Skalicky, C. Barbatti, Z. Fan, and M. Jarrett, *J. Alloy. Compd.*, 862, 158008 (1) ((2021).
- A.L. Greer, *Solidification and Casting* (Institute of Physics Publishing, Philadelphia, 2003), p 124.
- M. Johnsson, *Inter. J. Mater. Res.* 85(11), 781. (1994).
- Z. Fan, F. Gao, Y. Wang, H. Men, and L. Zhou, *Prog. Mater. Sci.*, 123, 100809 (2021).
- Y. Li, B. Hu, B. Liu, A. Nie, Q. Gu, J. Wang, and Q. Li, *Acta Mater.* 187, 51. (2020).
- D. Qiu, J.A. Taylor, M-X. Zhang, and P.M. Kelly, *Acta Mater.*, 55(4), 1447 (2007).
- K.M. Sree Manu, N.S. Barekar, J. Lazaro-Nebreda, J.B. Patel, and Z. Fan, *J. Mater. Process. Technol.*, 295, 117170 (2021).
- G.I. Eskin, *Ultrasonics Sonochem.* 1(1), S59. (1994).
- Y.W. Fu, G.L. Zhu, G. Zhong, and H. Nagaumi, *Mater. Sci. Forum* 877, 20. (2016).
- L. Bolzoni and N. Hari Babu, *Metall. Mater. Trans. A*, 50, 746 (2019).
- M. Nowak, L. Bolzoni, and N. Hari Babu, *Mater. Des.*, 66A 366 (2015).
- Y.H. Zhang, C.Y. Ye, Y.P. Shen, W. Chang, D.H. StJohn, G. Wang, and Q.J. Zhai, *J. Alloy. Compd.*, 812, 152022 (2020).
- L. Bolzoni and N. Hari Babu, *J. Mater. Res. Technol.*, 8(6) 5631 (2019).
- T. Smith, K. O'Reilly, and S. Kumar, *Metall. Mater. Trans. A* 44, 4866. (2013).
- A. Lui, P.S. Grant, and I.C. Stone, *Metall. Mater. Trans. A* 50, 5242. (2019).

21. A. Verma, S. Kumar, P.S. Grant, and K.A.Q. O'Reilly, ed. H. Weiland, A.D. Rollett, and W.A. Cassada, *ICAA13 Pittsburgh*, Cham: Springer, 2012). p. 1413.
22. S. Scharf, N. Bergedieck, E. Riedel, H. Richter, and N. Stein, *Sustainability* 12(16), 6457. (2020).
23. *Heat Treating of Aluminum Alloys*, ASM Handbook, Volume 4 (ASM International 1991), p 841-879.
24. B.S. Murty, S.A. Kori, and M. Chakraborty, *Inter. Mater. Rev.* 47, 3. (2002).
25. R. Nadella, D.G. Eskin, Q. Du, and L. Katgerman, *Prog. Mater. Sci.* 53, 421. (2008).
26. S.G. Shabestari, and M. Malekan, *J. Alloy. Compd.* 492, 134. (2010).
27. J.F. Grandfield, D.G. Eskin, and I.F. Bainbridge, *Direct-chill Casting of Light Alloys* (Wiley, New York, 2013), pp 144–155.
28. L. Bolzoni, M. Xia, and N. Hari Babu, *Sci. Rep.*, 6, 39554 (2016).
29. S.S. Dash, D.J. Li, X.Q. Zeng, and D.L. Chen, *J. Alloy. Compd.*, 870, 159413 (2021).
30. S. Chankitmongkong, S., D.G. Eskin, and C. Limmaneevichitr., *Metall. Mater. Trans. A*, 51, 467 (2020).
31. B. Milkereit, N. Wanderk, C. Schick, and O. Kessler, *Mater. Sci. Eng. A* 550, 87. (2012).
32. Information on www.thermocalc.com. Accessed 19 September 2021.
33. M.V. Glazoff, A.V. Khvan, V.S. Zolotarevsky, N.A. Belov, and A.T. Dinsdale, *Casting Aluminum Alloys. Their Physical and Mechanical Metallurgy*, (Oxford: Elsevier, 2019) p. 405-510.
34. J.H. Chen, E. Costan, M.A. van Huis, Q. Xu, and H.W. Zandbergen, *Science* 312(5772), 416. (2006).
35. C.D. Marioara, S.J. Andersen, T.N. Stene, H. Hasting, J. Walmsley, A.T.J. Van Helvoort, and R. Holmestad, *Philos. Mag.* 87(23), 3385. (2007).
36. G.H. Tao, C.H. Liu, J.H. Chen, Y.X. Lai, P.P. Ma, and L.M. Liu, *Mat. Sci. Eng. A* 642, 241. (2015).
37. W. Yang, L. Huang, R. Zhang, M. Wang, Z. Li, Y. Jia, R. Lei, and X. Sheng, *J. Alloy. Compd.* 514, 220. (2012).
38. J.B. Ferguson, H. Lopez, D. Kongshaug, B. Schultz, and P. Rohatgi, *Metall. Mater. Trans. A* 43, 2110. (2012).
39. J. Li, Q. An, S. Wu, F. Li, S. Lü, and W. Guo, *J. Alloys Compd.*, 808, 151771 (2019).
40. A. Smolej, B. Breskvar, M. Sokovic, V. Dragojevic, E. Slacek, and T. Smolar, *Aluminium* 78, 284. (2002).

Publisher's Note Springer Nature remains neutral with regard to jurisdictional claims in published maps and institutional affiliations.